JOURNAL OF Materials CHEMISTRY

# Some recent developments in mechanical activation and mechanosynthesis†

**Eric Gaffet,[a] Frédéric Bernard,[b] Jean-Claude Niepce,[b] Frédéric Charlot,[a,b] Christophe Gras,[a,b] Gérard Le Caër,*[c] Jean-Louis Guichard,[c] Pierre Delcroix,[c] Alain Mocellin[c] and Olivier Tillement[c]**

[a] *CNRS UPR 423, 'Nanomaterials' Group, IPSé, F-90010, Belfort Cedex, France. E-mail: Eric.Gaffet@utbm.fr.*
[b] *Laboratoire de Recherches sur la Réactivité des Solides, CNRS UMR 5613, Université de Bourgogne, UFR Sciences et Techniques, 9 Avenue A. Savary, BP 400, F-21011 Dijon Cedex, France*
[c] *Laboratoire de Science et Génie des Matériaux Métalliques, CNRS UMR 7584, Ecole des Mines, F-54042 Nancy Cedex, France. E-mail: lecaer@mines.u-nancy.fr*

***Received 13th April 1998, Accepted 18th June 1998***

After outlining the general characteristics of high-energy ball-milling, mechanochemical synthesis is argued to be an attractive method for the synthesis and transformation of materials. Phase transformations induced by milling, annealing of mechanically activated iron silicides, mechanically activated self-heat sustaining reactions (MASHS), for instance of FeAl, are first discussed. The route, which starts from mechanosynthesized powders to reach consolidated alumina–(Fe,Ti) composites, yields materials whose original morphologies and some mechanical properties are then described.

## 1 Introduction

Sophisticated methods most often spring to mind when thinking of means of mixing and combining elements in the solid state down to the atomic scale. Only a few people are aware that milling, a technique which was and still is mainly used for reducing the sizes of particles of various materials, is a possible method for this purpose. For a period of about thirty years, grinding has indeed been a method of synthesis of advanced materials and is called 'mechanical alloying' (MA).[1–5] Moreover, it is amusing that the repeated fracturing and rewelding processes of powder particles, which occur during milling (section 2.2) mix elements in a way reminiscent of chaotic transformations of the 'baker' type.[6,7] Mechanical alloying, which is basically a dry and high-energy milling process, is a powerful technique for synthesizing all kinds of materials[5] from metallic to ionic: extended solid solutions, alloys of immiscible elements, synthesis of alloys made from elements with widely different melting points, quasicrystals, amorphous phases, all sorts of compounds and composites. The synthesized materials, often with non-equilibrium structures, include, among others, crystalline materials with nanometer-sized grains,[8] with a typical average size of *ca.* 10 nm. Besides materials synthesis, high-energy ball-milling is a way of modifying the conditions in which chemical reactions usually take place either by changing the reactivity of as-milled solids (mechanical activation:[9–11] increase of reaction rates, lowering of reaction temperatures of ground powders) or by inducing chemical reactions during milling (mechanochemistry[9–11]). It is, furthermore, a way of inducing phase transformations in solids: amorphization or polymorphic transformations of compounds, disordering of ordered alloys,[2,3,5,8–19] *etc.* Mechanical alloying and grinding of materials are complex processes which depend on many factors, for instance on physical and chemical parameters such as the precise dynamic conditions, temperature, nature of the grinding atmosphere, chemical composition of the powder mixtures, chemical nature of the grinding tools,[19–31] *etc.* This may partly explain why the theoretical problem of predicting non-equilibrium phase transitions under milling is still under debate. After outlining the general characteristics of high-energy ball-milling (section 2), we describe how the previous means of mechanochemical synthesis, or mechanosynthesis, constitute attractive methods of materials transformations and of materials synthesis. Phase transformations induced by milling in oxides (section 3), mechanically activated annealing of transition metal silicides, mechanically activated self-heat sustaining reactions (MASHS) of FeAl (section 4) and the synthesis route from mechanosynthesized powders to consolidated alumina–(Fe,Ti) composites (section 5) will be discussed.

## 2 Typical ingredients of high-energy ball-milling

### 2.1 Milling equipment and experimental conditions

Experiments are performed in various types of high-energy mills, including for instance attrition mills (milling results from the stirring action of a rotating impeller with arms, horizontal in Fig. 1, which produce a relative movement between balls and powders), planetary and vibratory mills[30] (Fig. 1). Planetary mills, *e.g.* Fritsch P5 or P7, or mills G5 and G7 designed by Gaffet[31] (in which the rotation speeds of the vials, $w$, and of the disc, $W$, can be varied independently), vibratory (*e.g.* Spex 8000) mills and mills with control by an external magnetic field (designed by Calka and Radlinski[29]) are the most widely used in laboratories. In a planetary ball-mill (Fig. 1a), a rotating disc bears vials which rotate in the opposite direction. Both rotation speeds are of the order of several hundred rpm (the maximum rotation speeds $w_m$ and $W_m$ are 1000 rpm for the mills G5 and G7). In a vibratory mill like the Spex 8000 mill, the vial is shaken at a frequency of *ca.* 20 Hz in three orthogonal directions. The impact speed of the balls is of the order of several $m\,s^{-1}$ [22] and shock frequencies are several hundred Hz. Powders of the materials to be ground are introduced in the required proportions in a vial together with balls. Surface-active organic agents may be added to the powders to optimize the balance between welding and fracturing (see next section). They may give rise to a

†Basis of the presentation given at Materials Chemistry Discussion No. 1, 24–26 September 1998, ICMCB, University of Bordeaux, France.

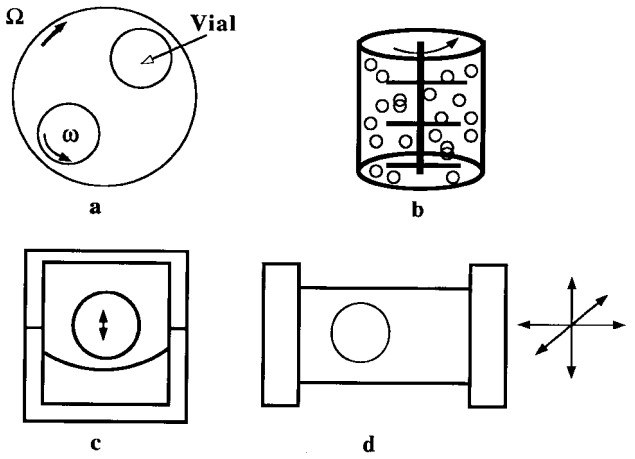


**Fig. 1** Various types of mills: (a) planetary mill, (b) attrition mill, (c) and (d) vibratory mills.

detrimental contamination of the ground powders by carbon. The vial is generally sealed in a glove box in various atmospheres (argon, nitrogen, air, *etc.*) or in vacuum. Nitrogen may however react with ground powders to form interstitial solid solutions or nitrides. Balls and vials are usually made of hardened steel, tungsten carbide, zirconia, *etc.* Besides the previous experimental conditions, other important experimental parameters include the number of balls, which depends on the mill and on the vial volume, the powder to ball mass ratio, which is typically of the order of 1/5 to 1/50, the minimum time which is needed to reach a final stationary state, and the milling temperature, which may be for instance conveniently varied in some vibratory mills.[16,21,22] The milling duration depends on a number of factors, including the type of mill used, the milling intensity, which sets for instance the rotation speeds $w$ and $W$ in a planetary mill, the milling mode (friction or direct shock) and the milling temperature. The duration typically amounts to some tens of hours for most high-energy ball-mills. Le Brun *et al.*[20] have modelled the MA process in planetary mills as a function of $w/W$. They conclude that most commercial mills operate in a mode which involves friction on the inner wall of the vial and not impact.

### 2.2 Process description

Fig. 2 compares the typical powers involved in various processes applied to solid materials.[31] Ball-milling is seen to cover a convenient range of injected powers. In the MA process of ductile powder mixtures of A and B, particles are trapped between colliding balls or between ball and vial and are subjected to a severe plastic deformation, which exceeds their mechanical strength, accompanied by a temperature rise.

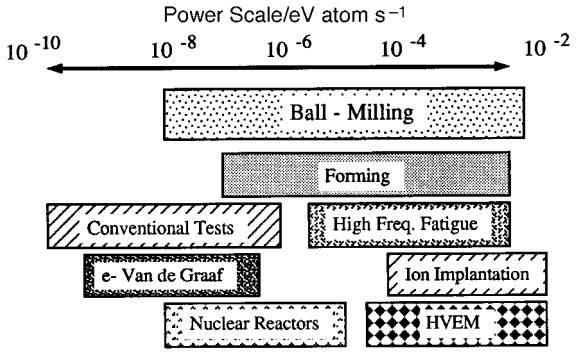


**Fig. 2** Comparison between typical ranges of injected powers in solid materials for some conventional mechanical tests, various irradiation processes and for ball-milling [P5 (Fritsch) and G5, G7 (Gaffet[31]) are planetary mills, Spex 8000 and Pulv.0 (Fritsch) are vibratory mills].

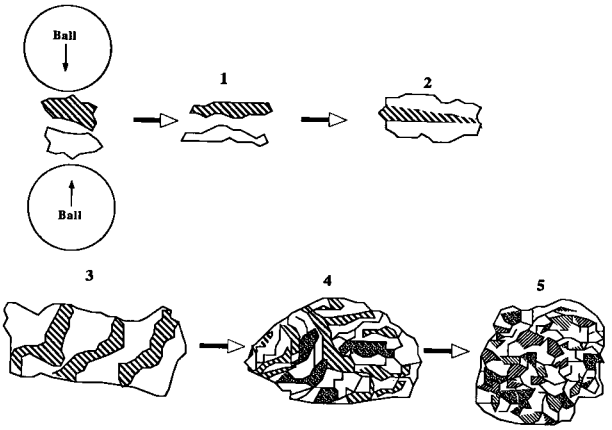


**Fig. 3** Stages of powder evolution during mechanical alloying of a mixture of A (white) and B (hatched) with progressive convolution of lamellae and combination of A and B.

During collisions, powder particles are subjected to high stresses (of the order of 200 MPa for steel balls in a Spex mill[2]) for times of the order of microseconds.[2] The waiting period between such efficient trapping events is typically of the order of tens to hundreds of seconds.[2,25,26] Particles are repeatedly flattened, fractured and welded. Fracture and welding are the two basic events which produce a permanent exchange of matter between particles and ensure mixing of the various elements of ground powders. A layered structure of A and B is thus formed and progressively refined and convoluted. Five typical stages of evolution of ductile powder mixtures are shown in Fig. 3. A balance between coalescence and fragmentation is achieved during MA which leads to a rather stable average particle size. The mixture of constituents finally becomes homogeneous and the elements are mixed on the atomic scale. In the case of brittle materials,[32] the temperature rise of the powder surface plays a major role and thermal activation is required for MA to occur. In the latter case, a granular-type microstructure is observed. The temperature rise, $\Delta T$, of metallic powders during MA is believed to be less than 300 K.[32]

Mechanical alloying of mixtures of powders of pure elements or of powders of already partially combined elements must be distinguished from the grinding of materials whose chemical composition remains the same during milling but whose structure is expected to evolve. They may lead to distinct end products whose nature depends on the various parameters of such synthesis and transformation processes, *i.e.* as previously mentioned, the powder to ball mass ratio, the milling duration, the milling temperature. Kinematic analyses have considered average shock energies, average shock frequencies[24] or ball momenta[21] to define dynamic parameters characterizing a milling experiment which are expected to be relevant for most mills. They lead to the definition of dynamic phase diagrams which describe, for a given milling temperature, the various phases which may be expected to form from an initial powder mixture according to the milling conditions.

### 2.3 Materials

As outlined in the introduction, all kinds of materials, almost without restriction, from metallic to ionic have been or may be synthesized or transformed by high-energy ball-milling. Numerous papers and patents report the synthesis of materials with improved mechanical, magnetic or catalytic properties. Crystalline materials synthesized by ball milling have grain sizes generally in the range from *ca.* 5–30 nm. Most often, for instance in metallic materials, the average size of as-milled powder particles is however not in the nm range but is typically micronic or submicronic. Every powder particle includes many

nanograins and may therefore be considered as a textureless polycrystal with a high density of grain boundaries. The crystallite size decreases rapidly with milling time but reaches a saturation value with prolonged grinding. The latter is explained for instance in face-centered cubic metals by the very high stress (Hall–Petch relation) which would be needed to deform them plastically *via* dislocation motion, as well as by the rate of recovery during milling. Besides nanograined materials prepared for instance by a direct combination of ground elemental powders or simply by grinding an already formed compound, attractive materials can also be obtained from chemical reactions which take place between ground reactants at temperatures and at rates at which they would normally not occur.[4,9–11] Some reactions, for instance the mechanochemical reduction of $SmCl_3$:[11]

$$SmCl_3 + 3Na \rightarrow Sm + 3NaCl$$

which would never occur at elevated temperatures due to unfavourable thermodynamical conditions, are even rendered possible. Mechanochemical reactions may be put to work to prepare dispersions of nanometric grains within matrices, yielding for example useful magnetic materials such as rare earth permanent magnet alloys like $SmCo_5$.[11] Redox or displacement reactions like:

$$\text{oxide or chloride of A} + \text{B} \rightarrow \text{oxide or chloride of B} + \text{A}^{9-11}$$

(for instance, A = Ti, V, Cr, Fe, Ni, Cu, Zn, Zr, Ta, Gd, Er, Sm; B = Na, Mg, Al, Si, Ca, Ti, Ni) have been used recently to prepare ultrafine magnetic metal powders with promising applications (recording media, ferrofluids, nanocomposite magnets), quantum dots, cermets, *etc.*[11,33–35] (section 5). If needed, the A compound can be replaced by a mixture of compounds of A1, A2, *etc.*, to form for instance alloys of A1, A2, *etc.*, dispersed in the final matrix (section 5). Mechanosynthesis offers thus supplementary degrees of freedom in the choice of possible routes for synthesizing new materials. Some possibilities offered by high-energy ball-milling in the fields of phase transitions induced by milling, mechanical activation and mechanochemical reactions are described below.

## 3 Effect of milling modes on far-from-equilibrium phase transitions induced by ball-milling in oxides

### 3.1 Some previous literature results

In the sixties, lead monoxide, PbO, was the most investigated oxide to show the effect of grinding on phase transitions. It exhibits two crystallographic structures which may be obtained not only by varying the temperature and pressure but also by changing the nature of applied stresses (hydrostatic or shear stresses). Lead monoxide exists in two polymorphic forms: a red (R) tetragonal modification (litharge: R-PbO) which is stable below 860 K, and a yellow (Y) orthorhombic modification (massicot: Y-PbO) which is stable at high temperature,[36] but may readily be stabilized at room temperature. Commercially available PbO is usually a mixture of both.[37] According to previous work, the martensitic transformation from Y-PbO to R-PbO may be driven by shear stresses and has been reported to take place during comminution.[38,39] The reverse transformation has been investigated by Dachille *et al.*[41] In 1961, White *et al.*[37] stated that a transformation of litharge into massicot occurs at temperatures higher than 813 K and at pressures higher than 0.6 GPa. The latter transformation was reported to be quite sluggish at low temperature while the reverse transformation is fast. On grinding, there is only a partial conversion of litharge to massicot or of massicot to litharge. Dachille *et al.*[40] concluded that shear forces do not modify equilibrium and affect only the rate at which it is reached. It was reported that shear stresses applied to litharge would convert it to massicot at room temperature only for pressures higher than the equilibrium pressure required by the *T*–*P* diagram. This was the case for their milling conditions as they estimated from various experiments that pressure pulses applied during milling ranged from about 1–2 GPa. Massicot is converted to litharge at room temperature at pressures lower than the equilibrium values by the action of displacive shears and is not transformed into the stable phase without shearing. In 1969, Lewis *et al.*[42] reported that the end ground product is a mixture of the two polymorphs. The fraction of each phase depends on the microstrain energy required to overcome the energy barrier for transformation, and on how shear stresses applied during milling modify the pressure–temperature phase diagram.[42] The influence of the type of applied stress, and thus of the milling mode, is further shown by the experiments described below.

### 3.2 Some recent literature results

Recent investigations have dealt with phase transitions induced by ball-milling in all kinds of oxides[43–45] (Table 1–3). The effects of milling conditions on the end ground products have been investigated in many metallic systems. The influence of the injected shock power on the crystal to amorphous phase transition is particularly well understood in the case of grinding of Ni–Zr intermetallic compounds.[46–48] Such a process has also been shown to be a suitable process for the preparation of nanocrystalline and amorphous semiconducting materials such as Si,[49,50] Ge,[51] Si–Ge.[52–54]

Still better control of milling parameters and better descriptions of ball kinematics inside containers of various mills are required for a deeper understanding of mechanically induced phase transitions. Experimental studies, such as the recent one which compares the formation of nanophases which occurs during surface wear induced by friction and during mechanical attrition of a pearlitic steel,[55] are also needed for further progress.

## 4 Mechanical activation

### 4.1 Mechanically activated annealing processing

Silicide synthesis by mechanical alloying of elemental powder mixtures is strongly affected by the generally high level of contamination coming from grinding tools. Such a problem may for instance be overcome by the addition of a grinding agent, which may however also produce an unwanted contamination. In the early 1990s, an alternative method to overcome this problem was proposed by Malhouroux-Gaffet and Gaffet, and was named mechanically activated annealing processing (M2AP). Such a solid state processing method, which combines short duration mechanical alloying and low temperature annealing, has been successfully applied to the syntheses of $FeSi_2$,[56] $MoSi_2$[57] and $WSi_2$.[58]

Starting from a mixture of elemental powders, the first M2AP milling step is basically a solid state mixing process due to chaotic processes (fracture + welding), with limited chemical combination of elements, which leads to the formation of micrometer-sized powders which contain nanoscale 3-D polyinterfaces between the elemental components (Fig. 3). In mechanical activation studies, the solid state reaction which forms the target phases occurs only during the subsequent annealing step.

The effect of milling conditions on grain sizes and the residual stresses were reported to modify the phase transformation kinetics induced by the final low temperature isothermal annealing. M2A processing has been found to be an efficient method for preparation of nanocrystalline materials in the Mo–Si and W–Si systems.

The influence of milling conditions on the M2A end product has been extensively investigated[56] in the case of the Fe–Si system. Phase transformations depend on annealing tempera-

**Table 1** Phase transformations induced by milling in some oxides[44–45] for an injected mechanical shock power of 1.1 W $g^{-1}$

| Oxide formula | Structure type before milling | Volume per formula unit/Å$^3$ | Structure type after milling | Volume per formula unit/Å$^3$ |
|---|---|---|---|---|
| $GeO_2$ | quartz | 40.3 | rutile | 27.6 |
| $TiO_2$ | anatase | 34.1 | rutile | 31.2 |
| $ZrO_2$ | baddaleyite | 35.2 | fluorite | 32.8 |
| $Dy_2O_3$ | C-type (bixbyte) | 75.9 | B-type (monoclinic) | 69.0 |
| $Y_2O_3$ | C-type | 74.5 | B-type | 67.6 |
| $Er_2O_3$ | C-type | 73.3 | B-type | 66.3 |
| $Yb_2O_3$ | C-type | 71.1 | B-type | 63.7 |

**Table 2** Formation of cubic zirconia phases by mechanical alloying[44,45] (injected shock power of 0.5 W $g^{-1}$)

| Initial state | End product | Coherence length/nm |
|---|---|---|
| 0.8 $ZrO_2$ + 0.2 CaO | $Ca_{0.2}Zr_{0.8}O_{1.8}$ (fluorite) | 13 ± 4 |
| 0.6 $ZrO_2$ + 0.2 $CaZrO_3$ | $Ca_{0.2}Zr_{0.8}O_{1.8}$ (fluorite) | 14 ± 4 |
| 0.8 $ZrO_2$ + 0.1 $Y_2O_3$ | $Y_{0.2}Zr_{0.8}O_{1.8}$ (fluorite) | 14 ± 4 |
| 0.8 $ZrO_2$ + 0.2 MgO | $Mg_{0.2}Zr_{0.8}O_{1.8}$ (fluorite) | 15 ± 4 |

**Table 3** Powder composition and experimental conditions leading to amorphous phases by mechanical alloying[44,45]

| Starting composition | Injected power/ W $g^{-1}$ | Milling duration/ days | End product |
|---|---|---|---|
| $Al_2O_3$ 62 mol%, $ZrO_2$ 38 mol% | 0.46 | 3 | amorphous + α-alumina (traces) |
| $Al_2O_3$ 62 mol%, $ZrO_2$ 35 mol%, $Y_2O_3$ 3 mol% | 0.46 | 3 | amorphous + α-alumina (traces) |
| $Al_2O_3$ 60 mol%, $ZrSiO_4$ 40 mol% | 0.46 | 10 | amorphous |
| $ZrSiO_4$ | 1.13 | 10 | amorphous |
| $ZrO_2$ 80 mol%, MgO 20 mol% | 0.46 | 7 | amorphous phase + cubic zirconia |

tures and on Fe crystallite sizes which depend in turn on milling conditions. They are: (i) for large Fe crystallites: Fe + Si→$Fe_xSi_{1-x}$ (300 °C)/FeSi + α-$FeSi_2$ (500 °C)/FeSi + β-$FeSi_2$ (800 °C); (ii) for small Fe crystallites: Fe + Si→FeSi (300 °C)/FeSi + β-$FeSi_2$ (500 °C)/FeSi + β-$FeSi_2$ (800 °C).

According to the previous experimental results, M2AP is a very suitable powder metallurgy process which allows the mastery of solid state reactions which occur for instance during reactive sintering processes. M2AP has also been found to be a very convenient method to produce nanocrystalline $MoSi_2$. Indeed, the first M2AP step leads to an activation of the three-dimensional distribution of the elements which react 400 °C below the temperature of the classical processes, *i.e.* 800 °C instead of 1200 °C.

### 4.2 Mechanically activated self heat sustaining reaction

More recently, mechanical activation has been successfully applied to self heat sustaining reactions (in short SHS reactions). The SHS synthesis is a process which results in a variety of compounds with large heats of formation. Once initiated by an ignition source, highly exothermic reactions become self sustaining and propagate through the reactant powder mixture, resulting within quite a short time in the formation of the end products.

The temperature reached just at the beginning of the reaction wave propagation is called the ignition temperature.

Such SHS reactions are characterized by fast moving combustion fronts (1–100 mm $s^{-1}$) and a self generated temperature varying from 1000–4000 K.

Processes which combine a first mechanical activation step and a SHS reaction have been named MASHS processing. This is an efficient way to synthesize nanocrystalline FeAl bulk materials with a grain size of 30–35 nm and a density of about 70–80% of the bulk value without a further compaction step (for a sample of several $cm^3$ in size).[59–61]

**4.2.1 Experimental.** 4.2.1.1 *Mechanically activated powders.* Pure elemental Al and Fe (10 g) were mixed together. Powder mixtures were sealed into a stainless steel vial, with a volume of 45 $cm^3$, together with 5 stainless steel balls (15 mm in diameter and 14 g in weight). The MA treatment was carried out for 4 h using a G5 planetary mill[31] (section 2.1).

*4.2.1.2 Compaction conditions.* Mechanically activated powders were cold compacted during 5 min in a rectangular die (20 × 10 × 10 $mm^3$) using a uniaxial press. Various experiments were performed with pressures ranging from 200 MPa to 2GPa.

*4.2.1.3 MASHS reaction.* A specially designed device was used for *in situ* experiments (for details, see ref. 59) to follow simultaneously the structural evolution of powders with a time resolved X-ray diffraction (TRXRD) system and the evolution of the surface temperature field using an imaging infrared camera. The vacuum tight, high temperature stainless steel chamber was filled with pure helium gas to prevent oxidation. It contained the alumina sample holder, which was centered at the goniometer axis, and an electrical heater. The compacted samples were ignited at one end by this resistively heated resistor, located on the sample holder.

**4.2.2 Results and discussion.** 4.2.2.1 *TRXRD patterns and related thermographic observations.* Typical TRXRD experiments consisting of 2048 scans each collected at 30 ms intervals, using a position sensitive detecting system developed for rapid data acquisition are exhibited in Fig. 4 and 5(a). The MASHS reaction leading to $MoSi_2$ phase formation is shown in Fig. 4. Fig. 5(a) and (b) are related to the synthesis of the FeAl intermetallic compound by the MASHS process. The thermal evolution of the sample surface during the thermal wave propagation induced by the MASHS process is shown in Fig. 5(b).

*4.2.2.2 Decrease of the ignition temperature induced by mechanical activation.* Table 4 gives the ignition temperature as a function of the milling conditions of the first activation step and of the compaction pressure which is used to prepare the green sample. Mechanical activation decreases the ignition temperature of the SHS reaction. Such an ignition temperature for Fe–Al powder mixtures prepared *via* a turbula route is equal to about 550 °C. The turbula ignition temperature is found to be 200 °C higher than that reached for mechanically activated powders.

*4.2.2.3 Effect of the mechanical activation mode (friction or direct shock) on the ignition temperature.* Using a G5 planetary mill[46–62] (section 2.1), it is furthermore possible to select a

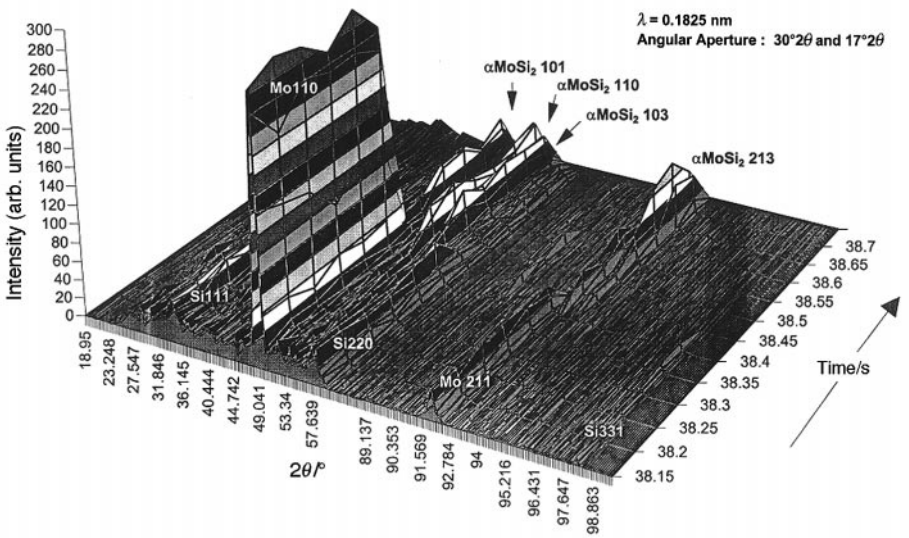


**Fig. 4** Time resolved X-ray diffraction patterns of the MASHS reaction: $Mo + 2Si \rightarrow MoSi_2$ (the experiment was performed with the synchrotron radiation facility at LURE/Orsay).

friction mode or a direct shock mode to activate the powders during the initial step of the MASHS process. As shown in Table 4, our experiments demonstrate that the friction mode is more efficient in decreasing the ignition temperature than the direct shock mode. We conclude that mechanical activation depends on the mode of transfer of mechanical energy to ground powders. It constitutes thus a very flexible way of influencing phase transformations. Experimental results call for more refined models to understand in detail such processes.

## 5 From mechanochemical reactions to materials: the case of alumina–metal composites

Brittle ceramics can be strengthened and toughened by the incorporation of various reinforcements. Ductile metallic reinforcement appears to be one of the most promising toughening mechanisms. It has already been investigated and the enhancement is mainly contributed by plastic inclusions which bridge the advancing crack. They are stretched as the crack opens until they fracture or separate from the matrix.

Two main difficulties with metal–ceramic composites still remain and restrict their use for structural applications: poor interfacial cohesion between particles and the ceramic matrix, and highly non-uniform and large metallic particles dispersions often associated with a high pore content.

Concerning the metallic particulate dispersion in ceramic oxides, the main limitation to toughening is often related to the weak bonding at the metal/ceramic interface. The metal particles are so weakly bonded to the oxide matrix that they easily pull free as the crack approaches. Then there is almost no plastic contribution to the toughness.

In order to overcome this problem, it has been proposed to design a complex metallic microstructure. Sun *et al.*[63] have studied $Al_2O_3$–Ni composite materials with two different microstructures, *i.e.* a dispersion distribution and a network distribution of nickel particles in the alumina matrix. The fracture toughness of the composite with a network is much higher than that of the composite with a microstructure of dispersed particles. For the network microstructure composite, the gauge length of the ductile phase is much larger, allowing the ductile nickel to stretch to failure between the crack planes.

Recently we have also proposed a new processing route to prepare alumina–metal composites with complex metal inclusion geometries and a resulting enhanced toughness. Nanostructured alumina–iron powders have been synthesized by high energy dry ball milling[33] and then consolidated by hot-pressing.[34] $\alpha$-$Al_2O_3$–Fe composite materials, for example, offer fine interwoven microstructures and metal particles with complex morphologies,[35] *e.g.* the cross-sections of metal inclusions have a fractal dimension of 1.76.

In these $\alpha$-$Al_2O_3$–Fe composite materials however the effective use of the plastic deformation of the iron phase can still be improved, in particular through an increase of the metal–ceramic interface bonding strength. It is common practice for interface strength adjustment to introduce a degree of interfacial chemical reaction. This can be achieved *via* specific different additives.[64] The presence of alloying elements in a metal can have a large effect not only on the surface energy of the matrix but also on the phenomena taking place at the alloy/ceramic interface.[65]

Focusing on the interface strength of alumina–metal composites, it is known to be quite difficult to obtain satisfactory bonding. The basic reason for this is the very different chemical characteristics of the alumina ceramic and the metal. Nevertheless it has been shown already that if a metal reacts with $Al_2O_3$ to form an interlayer, the joining of such metal to alumina can be significantly improved. The number of possible elements which can react with $Al_2O_3$ is very limited and titanium is one of the most important ones which falls into this category.[66]

According to Zhang *et al.*,[67] the interface bonding between $Al_2O_3$ and Ni can be improved by the presence of Ti. Segregation of Ti and formation of $Ti_2O_3$ at the interface cause a decrease of the interface energy between Ni and sintered $Al_2O_3$. Although in such a case, the rupture strength and the fracture toughness have not been enhanced, the addition of titanium has strongly modified the interfacial bonds.

We propose in this work to investigate the effect of titanium addition on some structural characteristics of mechanosynthesized $\alpha$-$Al_2O_3$–Fe cermets.

### 5.1 Experimental procedures

**5.1.1 Sample preparation.** The starting powders were commercially available aluminium (Ecka AS 011), titanium oxide (anatase from Aldrich) and iron oxide (hematite from Riedel de Haen). Average particle sizes of these powders were in the micrometer range. The as-received atomized aluminium was oxidized on its surface and the typical alumina content was 0.5–1 wt.%. The stoichiometric reactions which are expected

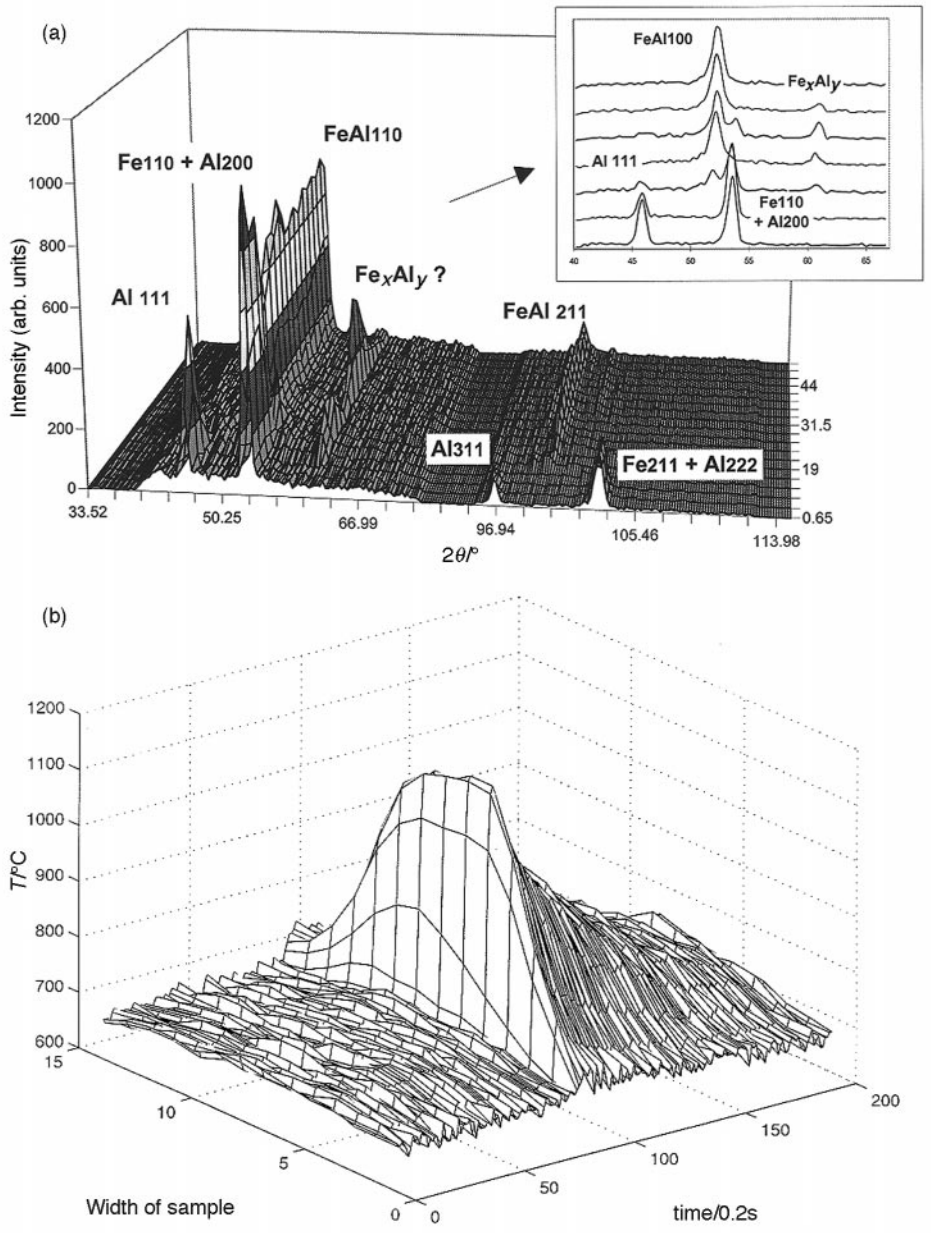


**Fig. 5** FeAl formation induced by a MASHS reaction: (a) time resolved synchrotron X-ray diffraction (LURE/Orsay), (b) time resolved infrared surface observations evidencing the propagation of a self heat sustaining reaction wave.

**Table 4** Effect of the milling mode (friction or direct shock) and of the compaction pressure on the ignition temperature

| | Friction mode | | | Shock mode | | |
|---|---|---|---|---|---|---|
| *P*/MPa | 350 °C | 400 °C | 450 °C | 350 °C | 375 °C | 450 °C |
| 100 | | No | No | | | |
| 200 | Yes | Yes | Yes | No | Yes | Yes |
| 600 | No | Yes | Yes | No | No | Yes |
| 2000 | No | No | Yes | No | No | No |

to take place during the ball-milling are:

$$2\ Al + Fe_2O_3 \rightarrow Al_2O_3 + 2\ Fe \quad (1)$$

and with the addition of elemental Ti:

$$2\ Al + 0.87\ Fe_2O_3 + 0.195\ TiO_2 \rightarrow Al_2O_3 + 1.95\ (Fe_{0.9}Ti_{0.1}) \quad (2)$$

Both correspond to a volume fraction of metallic phase of about 36%. It is important to point out that the former of these reaction schemes has indeed been found to take place with hercynite $FeAl_2O_4$ as an intermediate.[33] The latter however was somewhat speculative, and it is one objective of the present paper to provide some experimental evidence about the course followed by the titanium bearing species both during milling and the subsequent high temperature densification of the resulting powder.

High energy milling was carried out in a planetary ball-mill (Fritsch Pulverisette 5). Grinding utensils (15 balls of 20 mm diameter and vials) were made from hardened chromium steel. The different stoichiometric mixtures were milled during 4 h with a powder-to-ball ratio of 1 to 10.

Because of particle welding during high energy milling, some relatively large agglomerates formed (*ca.* 20 μm diameter). Therefore, before sintering, the powders were subsequently wet-milled in THF for 2 h. The mean particle size was thus reduced to 1.7 μm after dispersion in propan-2-ol with ultrasonication. The resulting slurry was dried with a rotary evaporator. Then the powder was vacuum hot-pressed in a graphite die heated to 1700 K. The selected sintering cycle was an initial pressureless heating to 1000 K (10 K $min^{-1}$) followed by

heating under a constant 30 MPa applied pressure to 1700 K (30 K $min^{-1}$) with a hold time of 30 min at this temperature.

**5.1.2 Sample characterisation.** The as-milled products have been characterized by X-ray diffraction (XRD) using Co-Kα radiation ($\lambda = 0.17889$ nm), scanning electron microscopy (SEM; JEOL JSM 6400F), transmission electron microscopy (TEM) and electron microprobe analysis. Density measurements using Archimedes' principle were made on the as-sintered samples which also were prepared for microstructural characterization using standard techniques. From the as-pressed discs (5 mm high by 30 mm diameter), dense bars were cut. The machining damage was removed mechanically by polishing, ultimately with 1 μm diamond paste to produce an optical finish.

The microstructures were observed by high-magnification optical microscopy (Reichert-Jung) and SEM. The surfaces were coated with gold to avoid charging during SEM observations. No etching was necessary to show morphological aspects of iron dispersion since the contrast between both phases was sufficient.

$^{57}$Fe Mössbauer spectra of as-milled powders and of powders from consolidated cermets were obtained in transmission geometry at room temperature using a *ca.* 15 mCi source of $^{57}$Co in Rh. The spectra were analyzed by a method[68] that extracts a hyperfine magnetic field distribution (HMFD) $P(H)$ from an experimental spectrum [$P(H)\Delta H$ is the fraction of iron atoms whose field is between $H$ and $H+\Delta H$, here $\Delta H =$ 2 kG]. The $^{57}$Fe isomer shifts are given with respect to α-Fe at room temperature.

### 5.2 Results and discussion

**5.2.1 As-milled powders.** Fig. 6 shows the morphology and microstructure of typical mechanosynthesized powder particles. After such reactive milling, nanometer-sized crystallites are produced from the initial micrometer-sized powders. The particles consist of finely divided aggregates of crystallites 2–30 nm in size with presumably an extremely high defect density due to the mechanical action and the powder nanostructure. The mean crystallite size, as estimated by X-ray line broadening and TEM photographic observations, is about 10 nm for both the α-$Al_2O_3$ and the metal phases. No differences between Fe/α-$Al_2O_3$ and Fe–Ti/α-$Al_2O_3$ composite powder morphologies were observed. The corresponding particles appear as a very fine-scale homogeneous assembly of α-$Al_2O_3$ and α-Fe or some α-(Fe–Ti) alloy. Fig. 7(a) shows a room-temperature $^{57}$Fe Mössbauer spectrum of an as-milled Fe–Ti/α-$Al_2O_3$ composite powder with an initial composition given by reaction (2). The main contribution to the spectrum is associated with a magnetic bcc Fe-rich alloy. Besides the external peaks of the main sextuplet, at *ca.* $\pm 5.3$ mm $s^{-1}$, intense shoulders are seen at $\pm 5$ mm $s^{-1}$. The corresponding isomer shifts are both $0.00 \pm 0.01$ mm $s^{-1}$. The two larger hyperfine fields measured from the hyperfine field distribution $P(H)$ are $331 \pm 1$ kG and $309 \pm 1$ kG respectively. A hyperfine field of about 331 kG is expected for Fe atoms Fe(0,0) which have no T = Ti atom first-nearest (NN) or next nearest neighbour (NNN) in an Fe-rich bcc Fe–Ti alloy,[69] or more generally for Fe(0,0) in many Fe–T alloys with low solute contents. Hyperfine fields of 309 and 311 kG are predicted for Fe atoms which have one Ti NN or NNN respectively.[69] Hyperfine fields which are smaller by only a few kG would however be observed for Fe atoms with one Al or Cr NN respectively. The latter element may come from a contamination of ground powders by steel from the milling tools. Much less intense shoulders are observed however on Mössbauer spectra of as-milled Fe/α-$Al_2O_3$ composite powders[33] with the same volume fraction of metal. Assuming a random distribution of solute atoms in $Fe_{1-x}T_x$, the solute contents may be calculated from

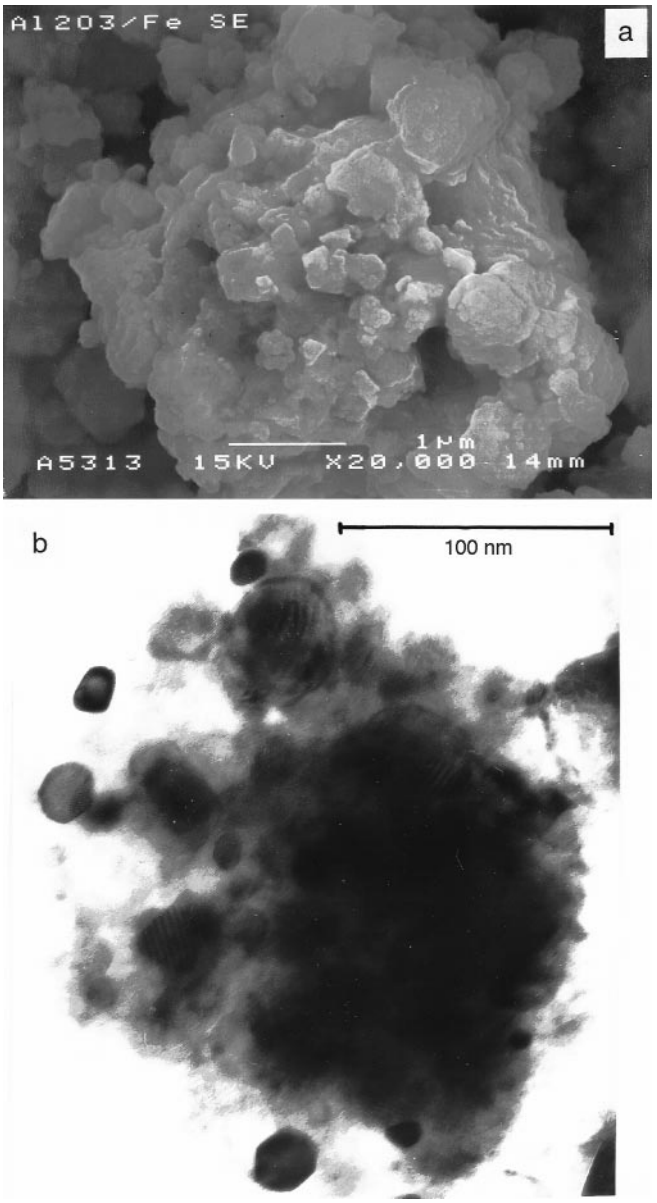


**Fig. 6** Morphologies of α-$Al_2O_3$/Fe powders (SEM and TEM).

the relative area of the Fe(0,0) peak of the hyperfine field distribution $P(H)$ which is equal to the 14th power of $(1-x)$, as the only significant hyperfine field changes are due to the first and second NN. We obtain $x = 0.08 \pm 0.01$ from $P(H)$ while $x$ is at most about 0.02 in the absence of titanium. Mössbauer spectroscopy confirms thus the formation of an alloy with a larger solute content in Fe–Ti/α-$Al_2O_3$ than in Fe/α-$Al_2O_3$ as-milled powders. The Ti content of the metallic phase is in any case less, by about 0.02–0.04, than the nominal composition $Fe_{0.9}Ti_{0.1}$ expected from reaction (2). It is thus reasonable to assume that some amount of titanium is still contained in oxide phases. In equilibrium conditions, the Ti solubility in α-Fe is at most 0.10 at 1566 K while it is less than 0.06 below *ca.* 1300 K.[70] Although the Fe–Ti alloy is not formed in equilibrium conditions during the mechanochemical reaction, the occurrence of a significant temperature rise cannot be ruled out. A small peak is seen in the middle of the Mössbauer spectrum at a slightly negative velocity [Fig. 7(a)]. Part of it is associated with an even smaller peak located at *ca.* 2 mm $s^{-1}$. Similar features were reported for Fe/α-$Al_2O_3$ as-milled powders[33,71] and were attributed both to clusters of Fe atoms in α-$Al_2O_3$ and to hercynite $FeAl_2O_4$. The Fe fraction in the latter phases, estimated from the spectrum of Fig. 7(a), is *ca.* 2–3% of the total Fe amount. We notice that most Fe

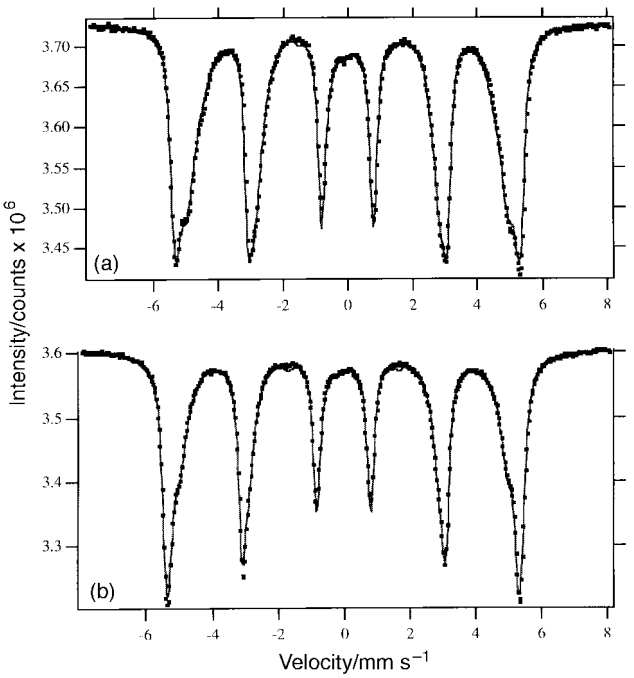


**Fig. 7** Room-temperature $^{57}$Fe Mössbauer spectra of (a) as-milled Fe–Ti/α-$Al_2O_3$ composite powders, (b) powders from as-sintered Fe–Ti/α-$Al_2O_3$ composites.

atoms implanted in α-$Al_2O_3$ are stabilized in the form of fine particles of α-Fe,[72] a result which further emphasizes analogies found sometimes between ion implantation and mechanical alloying (Fig. 2). In both techniques, forced atomic jumps compete with thermal jumps to determine the final state of the investigated materials.[6]

**5.2.2 As-sintered samples.** Densification upon sintering begins for each composition above 1200 K (Fig. 8). The influence of titanium on densification is small in the lower temperature region. However, this influence becomes noticeable around 1450 K, slowing the sintering process. Nevertheless, the final overall shrinkage remains the same and both samples achieved a final density of about 98% of theoretical.

Typical micrographs of both composite microstructures are shown in Fig. 9. The metallic areas have bright contrast, the alumina grains are grey. There is no metal concentration gradient between the surface and the core of the pellets and the metal content is almost the same everywhere. The metallic inclusion morphology is very interpenetrating and ramified.

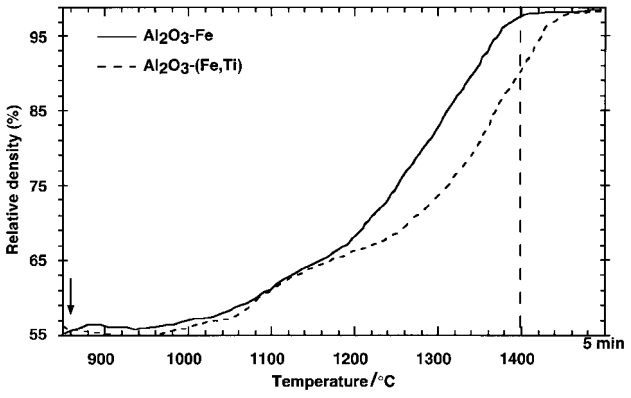


**Fig. 8** Sintering kinetics of α-$Al_2O_3$/Fe composites with and without addition of Ti (right of the dashed vertical line: relative density as a function of time at 1400 °C, a constant density is reached in both cases after 5 min).

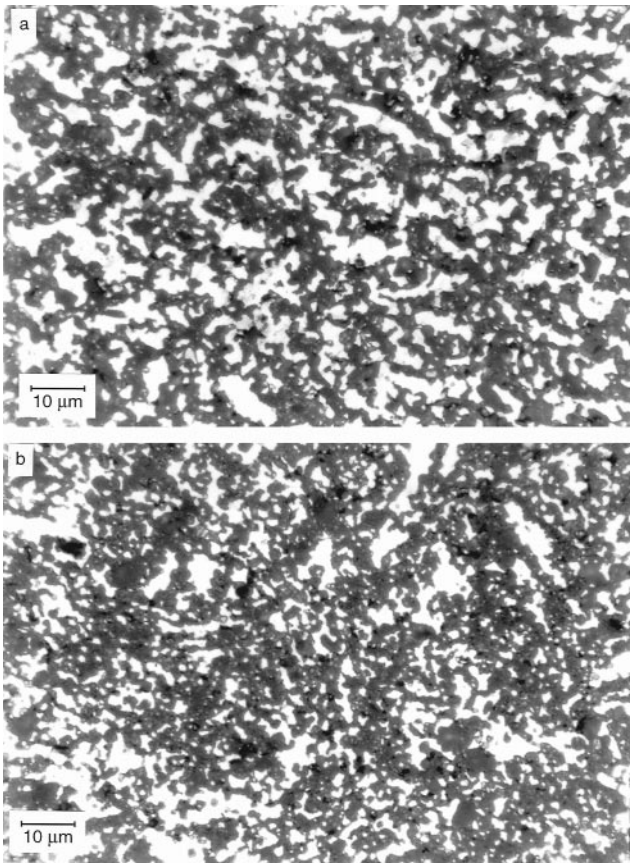


**Fig. 9** Optical micrographs of α-$Al_2O_3$/Fe and α-$Al_2O_3$/(Fe,Ti) composite microstructures.

The particles with such a shape seem to be firmly bonded to the ceramic matrix. Residual pores mostly located at metal/ceramic interfaces, are not observable in Fig. 9 and no obvious difference between the Ti-free and Ti-containing materials is noted either at such a magnification. Quantitative image analysis, however, reveals differences in the respective particle size distributions. For the Fe–Ti/α-$Al_2O_3$ composites, the metallic particles with a submicrometer size represent 68% of the total number of metallic particles instead of only 55% for the case of pure iron–alumina composites

To obtain more information about the titanium distribution, a Mössbauer spectrum of Fe–Ti/α-$Al_2O_3$ powders collected from a consolidated sample was recorded [Fig. 7(b)]. It shows qualitative features similar to those of the spectrum of Fig. 7(a). The relative fraction of the central component has decreased to *ca.* 1% of the total Fe amount. The largest change is seen for the bcc Fe-based alloy. The solute content calculated in a way similar to that described in the previous section decreases to $0.035 \pm 0.005$. As no other spectral contribution appears in Fig. 7(b), it must be concluded that the solute atoms lost by the α-Fe phase are from phases which do not contain significant amounts of Fe. The chemical compositions and the structures of the latter phases will have to be investigated by other methods to determine their possible influence on the properties of the Fe–Ti/α-$Al_2O_3$ consolidated cermets.

Finally, during thermal treatment up to 1875 K, *i.e.* above the metallic phase melting point, the latter was found to exude. The wettability of the metallic phase on aluminium oxide is much affected by the presence of Ti. Fig. 10 shows that Fe has a poor wettability while (Fe,Ti) has a quite different behaviour. It is anticipated that such differences will be reflected upon properties of the respective materials, particularly the mechanical properties.

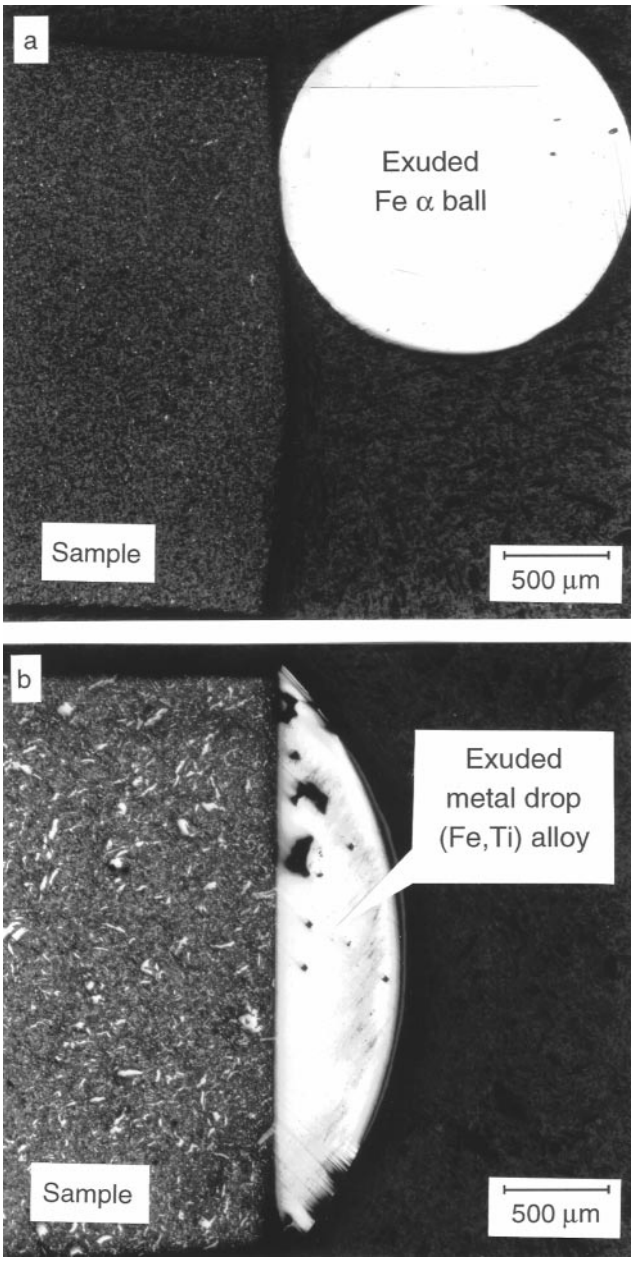


**Fig. 10** Optical micrographs of $\alpha$-$Al_2O_3$/Fe (a) and $\alpha$-$Al_2O_3$/(Fe,Ti) (b) composites after thermal treatment up to 1875 K.

## 6 Conclusions and perspectives

As outlined above, mechanosynthesis has evolved significantly during the last 10 years by reaching for instance a better kinematic modeling of all kinds of mills. Such models have led, and will lead, to the design of new mills which allow control of the ball movements, shock energies and frequencies. Even more, they allow mastery of the components of friction and of direct shock during the interactions between balls and vial walls.

The activation of far-from-equilibrium phase transitions, named M2A processing, and of MASHS reactions allows definition of new ways of synthesizing nanomaterials which may exhibit some very intriguing properties. Noticeable are for instance the abnormal thermal expansion of Ni which is 20 times larger for nanocrystalline ball milled powders[73] than it is for coarse-grained Ni, or the changes of the corrosion mechanisms of mechanosynthesized nanocrystalline Ni coatings[74] as compared to their classical counterparts.

Alumina–iron and alumina–(iron–titanium alloy) cermets have been prepared by hot-pressing nanocomposite mechanosynthesized powders. The materials exhibit a homogeneous dispersion of Fe or (Fe,Ti) alloy which is simultaneously achieved at the nanometre and micrometre scales. Interwoven microstructures are observed. Different observations between Fe/$\alpha$-$Al_2O_3$ and Fe–Ti/$\alpha$-$Al_2O_3$ indicate that the initial objective of the synthesis of an alumina–metal composite with a complex metallic microstructure and a modified interface has been achieved.

Investigations performed over a period of about fifteen years provide realistic ideas about the actual potential of synthesis methods which involve mechanical energy and about the problems they raise. Mechanosynthesis is a promising synthesis route for all kinds of nanomaterials, often with original features, and a step towards the preparation of consolidated materials with improved properties. Milling must no longer be regarded only as a millenial method of powder processing but it must considered nowadays as being also a modern technique of preparation and transformation of materials.

F. C. thanks the 'Conseil Régional de Bourgogne' and the 'Conseil Géneral du Territoire de Belfort' for financial support. The authors thank J. C. Gachon (Université H. Poincaré, Nancy), M. Bessiere, M. Gailhanou (LURE/Orsay), M. Gramond (ECP) for help during the *in situ* SHS experiments performed in LURE/Orsay. A. M. thanks the EEC for financial support (Interreg 2).

## References

1 J. S. Benjamin, *Metall. Trans.*, 1970, **1**, 2943.
2 R. B. Schwarz, *Mater. Sci. Eng.*, 1988, **97**, 71; *Mater. Sci. Forum*, 1998, **269–272**, 665.
3 L. Schultz, *Philos. Mag. B*, 1990, **61**, 453.
4 J. J. de Barbadillo, *Key Eng. Mater.*, 1993, **77–78**, 187.
5 *Proceedings of the International Symposium on Metastable, Mechanically Alloyed and Nanocrystalline Materials (ISMANAM)*, *Mater. Sci. Forum*, 1995, **179–181**; 1996, **225–227**; 1997, **235–238**; 1998, **269–272**.
6 G. Martin and P. Bellon, *Metall. Sci. Technol.*, 1991, **9**, 61.
7 K. N. Ishihara, T. Matsumoto, A. Otsuki and P. H.Shingu, *Key Eng. Mater.*, 1995, **103**, 77.
8 A. R. Yavari, *Mater. Trans. JIM*, 1995, **36**, 228.
9 I. J. Lin, S. Nadiv and D. J. M. Grodzian Pavlyukhin, *Miner. Sci. Eng.*, 1975, **7**, 313.
10 V. V. Boldyrev, N. Z. Lyakhov, Yu. T. Pavlyukhin, E. V. Boldyreva, E. Yu Ivanov and E. G. Avvakumov, *Sov. Sci. Rev. B. Chem.*, 1990, **14**, 105.
11 G. B. Schaffer and P. G. McCormick, *Mater. Sci. Forum*, 1992, **88–90**, 779; *Appl. Phys. Lett.*, 1989, **55**, 45; P. G. McCormick, *Mater. Trans. JIM*, 1995, **36**, 228; T. Tsuzuki and P. G. McCormick, *Appl. Phys. A*, 1997, **65**, 607.
12 E. Hellstern, H. J. Fecht, Z. Fu and W. L. Johnson, *J. Appl. Phys.*, 1989, **65**, 305.
13 J. S. C. Jang and C. C. Koch, *J. Mater. Res.*, 1990, **5**, 325.
14 H. Bakker, G. F. Zhou and H. Yang, *Prog. Mater. Sci.*, 1995, **39**, 159.
15 L. B. Hong, L. Anthony and B. Fultz, *J. Mater. Res.*, 1995, **10**, 126.
16 P. Pochet, E. Tominez, L. Chaffron and G. Martin, *Phys. Rev. B*, 1995, **52**, 4006.
17 G. Le Caër, P. Delcroix, B. Malaman, R. Welter, B. Fultz and E. Ressouche, *Mater. Sci. Forum*, 1996, **225–227**, 589.
18 S. Gialanella, X. Amils, M. D. Baro, P. Delcroix, G. Le Caër, S. Lutterotti and S. Surinach, *Acta Mater.*, 1998, **44**, in press.
19 S. Bégin-Colin, G. Le Caër, M. Zandona, E. Bouzy and B. Malaman, *J. Alloys Compd.*, 1995, **227**, 157.
20 P. Le Brun, L. Froyen and L. Delaey, *Mater. Sci. Eng. A*, 1993, **161**, 75.
21 Y. Chen, M. Bibole, R. Le Hazif and G. Martin, *Phys. Rev. B*, 1993, **48**, 14.
22 D. Basset, P. Matteazzi and F. Miani, *Mater. Sci. Eng.*, 1994, **174**, 71.
23 M. Abdellaoui and E. Gaffet, *J. Alloys Compd.*, 1994, **209**, 351.
24 M. Abdellaoui and E. Gaffet, *Acta Metall. Mater.*, 1995, **43**, 1087.
25 T. H. Courtney, *Mater. Trans. JIM*, **36**, 1995, 110.
26 T. H. Courtney and D. Maurice, *Scr. Mat.*, **34**, 1996, 5.

27 M. Abdellaoui and E. Gaffet, *Acta Metall. Mater.*, 1996, **44**, 725.
28 A. Iasonna and M. Magini, *Acta Mater.*, 1996, **44**, 1109.
29 A. Calka and A. P. Radlinski, *Mater. Sci. Eng. A*, 1991, **134**, 1350.
30 *Metals Handbook*, Ninth Edition, vol. 7; Powder Metallurgy, American Society for Metals, Ohio, 1988.
31 E. Gaffet, M. Abdellaoui and N. Malhouroux-Gaffet, *Mater. Trans. JIM*, 1995, **36**, 198.
32 R. M. Davis, B. McDermott and C. C. Koch, *Metall. Trans. A*, 1988, **19**, 2867.
33 P. Matteazzi and G. Le Caër, *J. Am. Ceram. Soc.*, 1992, **75**, 2749.
34 J. L. Guichard, PhD thesis, INPL Nancy, France, 1998.
35 J. L. Guichard, O. Tillement and A. Mocellin, *J. Mater. Sci.*, 1997, **32**, 4513.
36 V. V Zyryanov, *Inorg. Mater.*, 1997, **33**, 1039.
37 W. B. White, F. Dachille and R. Roy, *J. Am. Ceram. Soc.*, 1961, **44**, 170.
38 I. J. Lin and S. Niedzwiedz, *J. Am. Ceram. Soc.*, 1973, **56**, 62.
39 G. L. Clark and R. Rowan, *J. Am. Ceram. Soc.*, 1941, **63**, 1302.
40 F. Dachille and R. Roy, *Nature*, 1960, **186**, 34.
41 F. Dachille and R. Roy, in *Reactivity of Solids*, ed. J. H. de Boers, W. G. Burgers, E. W. Gorker, J. P. F. Huesse and G. C. A. Schuit, Elsevier, Princeton, NY, 1961, pp. 502–511.
42 D. Lewis, D. O. Northwood and R. C. Reeve, *J. Appl. Crystallogr.*, 1969, **2**, 156.
43 S. Bégin-Colin, G. Le Caër and A. Mocellin, *Philos. Mag. Lett.*, 1994, **69**, 1.
44 D. Michel, F. Faudot, E. Gaffet and L. Mazerolles, *J. Am. Ceram. Soc.*, 1993, **76**, 2884.
45 D. Michel, L. Mazerolles, P. Berthet and E. Gaffet, *Eur. J. Solid State Inorg. Chem.*, 1995, **32**, 673.
46 E. Gaffet, *Mater. Sci. Eng. A*, 1989, **119**, 185.
47 E. Gaffet, *Mater. Sci. Eng. A*, 1991, **132**, 181.
48 E. Gaffet and L. Yousfi, *Mater. Sci. Forum*, 1992, **88–90**, 51.
49 E. Gaffet and M. Harmelin, *J. Less Common Met.*, 1990, **157**, 201.
50 T. D. Shen, C. C. Koch, T. L. McCormick, R. J. Nemanich, R. J. Huang and J. G. Huang, *J. Mater. Res.*, 1995, **10**, 139.
51 E. Gaffet, *Mater. Sci. Eng. A*, 1991, **136**, 161.
52 R. M. Davis and C. C Koch, *Scr. Metall.*, 1987, **21**, 305.
53 E. Gaffet, F. Faudot and M. Harmelin, *Mater. Sci. Eng. A*, 1991, **149**, 85.
54 B. B. Bokhonov, I. G. Konstanchuk and V. V Boldyrev, *J. Alloys Compd.*, 1993, **191**, 239.
55 G. Baumann, Y. Zhong and H. J. Fecht, *Nanostruct. Mater.*, 1996, **7**, 237.
56 N. Malhouroux-Gaffet and E. Gaffet, *J. Alloys Compd.*, 1993, **198**, 143.
57 E. Gaffet and N. Malhouroux-Gaffet, *J. Alloys Compd.*, 1994, **205**, 27.
58 E. Gaffet, N. Malhouroux-Gaffet, M. Abdellaoui and A. Malchere, *Rev. Metall.*, 1994, 757.
59 E. Gaffet, F.Charlot, F. Bernard and J. C. Niepce, *Mater. Sci. Forum*, 1998, **269–272**, 379.
60 F. Bernard, F. Charlot, E. Gaffet and J. C. Niepce, *Int. J. Self-Propag. High-Temp. Synth.*, in press.
61 F. Charlot, E. Gaffet, B. Zeghmati, F. Bernard and J. C. Niepce, *Mater. Sci. Eng. A.*, submitted.
62 E. Gaffet, *Mater. Sci. Eng. A*, 1991, **135**, 291.
63 X. Sun and J. A. Yeomans, *J. Mater. Sci*.,1996, **31**, 875.
64 J. M. Howe, *Int. Mat. Rev.*, 1993, **38**, 233.
65 S. A. Dregia and P. Wynblatt, *Acta Metall. Mater.*, 1991, **39**, 771.
66 J. V. Naidich, *Prog. Surf. Membr. Sci.*, 1981, **14**, 353.
67 X. Zhang, G. Lu, M. J. Hoffmann and R. Metselaar, *J. Eur. Ceram. Soc.*, 1995, **15**, 225.
68 G. Le Caër and J. M. Dubois, *J. Phys. E: Sci. Instrum*., 1979, **12**, 1083.
69 G. K. Wertheim, V. Jaccarino, J. H. Wernick and D. N. E. Buchanan, *Phys. Rev. Lett*., 1964, **12**, 24.
70 K. C. Hari Kumar, P. Wollarts and L. Delaey, *Calphad*, 1994, **18**, 223.
71 G. Cao, G. Concas, A. Corrias, R. Orru, G. Paschina, B. Simoncini and G. Spano, *Z. Naturforsch.*, *Teil A*, 1997, **52**, 539.
72 T. Kobayashi, A. Nakanishi, K. Fukumura and G. Langouche, *J. Appl. Phys.*, 1998, **83**, 4631.
73 M. Tachikart, E. Gaffet, Ph. Lesage, C. Meunier and S. Vives, *Scr. Mater.*, 1998, in press.
74 Eur. Feder Corr. Publications No. 20, *Organic and Inorganic Coatings for Corrosion Prevention—Research and Experiences*, Papers from Eurocorr'96, Institute of Materials, London, 1997.

*Paper 8/04645J*